Understanding the Australian Monsoon change during the Last Glacial Maximum with multi-model ensemble

Mi Yan[1,2], Bin Wang[3,4], Jian Liu[1,2*], Axing Zhu[1,2,5,6], Liang Ning[1,2,7] and Jian Cao[4]

1 Key Laboratory of Virtual Geographic Environment, Ministry of Education; State key Laboratory of Geographical Environment Evolution, Jiangsu Provincial Cultivation Base; School of Geography Science, Nanjing Normal University, Nanjing, 210023, China.

2 Jiangsu Center for Collaborative Innovation in Geographical Information Resource Development and Application, Nanjing, 210023, China.

3 Department of Atmospheric Sciences, University of Hawaii at Manoa, Honolulu, HI 96825, USA.

4 Earth System Modeling Center, Nanjing University of Information Science and Technology, Nanjing, 210044, China.

5 State Key Lab of Resources and Environmental Information System, Institute of Geographic Sciences and Natural Resources Research, Chinese Academy of Sciences, Beijing, 100101, China

6 Department of Geography, University of Wisconsin-Madison, Madison, WI 53706, USA

7 Climate System Research Center, Department of Geosciences, University of Massachusetts, Amherst, 01003, USA.

* Corresponding author address: Dr. Jian Liu, School of Geography Science, Nanjing Normal University, 1 Wenyuan Road, Nanjing 210023, China

E-mail: jliu@njnu.edu.cn

Abstract

25

26   The response of Australian monsoon to the external forcings and the related mechanisms

27   during the Last Glacial Maximum (LGM) are investigated by multi-model experiments in

28   CMIP5/PMIP3. Although the annual mean precipitation over the Australian monsoon region

29   decreases, the annual range, or the monsoonality, is enhanced. The precipitation increases in

30   early austral summer and decreases in austral winter, resulting in the amplified annual range, but

31   the main contribution comes from the decreased precipitation in austral winter. The decreased

32   winter precipitation is primarily caused by weakened upward motion, although reduced water

33   vapor has also a moderate contribution. The weakened upward motion is induced by the

34   enhanced land–sea thermal contrast, which intensifies the divergence over northern Australia.

35   The increased Australian monsoon rainfall in early summer, on the other hand, is an integrated

36   result of the positive effect of local dynamic processes (enhanced moisture convergence) and the

37   negative effect of thermodynamics (reduced moisture content). The enhanced moisture

38   convergence is caused by two factors: the strengthened northwest–southeast thermal contrast

39   between the cooler Indochina–western Indonesia and the warmer northeastern Australia, and the

40   east–west sea surface temperature gradients between the warmer western Pacific and cooler

41   eastern Indian Ocean, both due to the alteration of land–sea configuration arising from the sea

42   level drop. The enhanced Australian monsoonality in the LGM is not associated with global scale

43   circulation change such as the shift of the ITCZ, rather, it is mainly due to the change of regional

44   circulations around Australia arising from the changes in land-sea contrast and the east-west SST

45   gradients over the Indo-western Pacific oceans. This finding should be taken into account when

46   investigating its future change under global warming. Our findings may also explain why proxy

47   records indicate different changes in Australian monsoon precipitation during the LGM.

48

1 Introduction

The changes of the Australian monsoon are crucial for human society and ecology in Australia (Reeves et al., 2013a), considering the socio-economic importance of monsoon rainfall (Wang et al., 2017). As the monsoons of the summer hemisphere are linked via outflows from the opposing winter hemisphere, the Australian monsoon can also influence the Asian–Indonesian–Australian monsoon system (Eroglu et al., 2016). It is important to understand how and why the Australian monsoon would change in response to the global climate change.

With strong climatic forcings (including low greenhouse gas (GHG) concentrations, large ice-sheets, and low sea level, etc.), the Last Glacial Maximum (LGM) is one of the key periods that provides an opportunity to better understand the mechanisms of how global and regional climate respond to external forcings (Hewitt et al., 2001; Braconnot et al., 2007; Braconnot et al., 2011; Harrison et al., 2014). Previous studies have investigated how the external forcings and boundary conditions during the LGM affected the Intertropical Convergence Zone (ITCZ) (Broccoli et al., 2006; Donohoe et al., 2013; McGee et al., 2014), the Walker circulation (DiNezio et al., 2011), the Indo-Pacific climate (Xu et al., 2010; DiNezio and Tierney, 2013; DiNezio et al., 2016), the SH circulation (Rojas, 2013), and the global monsoon (Jiang et al., 2015; Yan et al., 2016). The Australian monsoon onset and variability during the post-glacial, the late deglaciation, and the Holocene have also been studied using proxy datasets (Ayliffe et al., 2013; De Deckker et al., 2014; Kuhnt et al., 2015; Bayon et al., 2017). However, due to the limitation of the scarce proxy datasets, the Australian monsoon change during the LGM is far from being clearly understood.

There are different proxy evidences indicating different Australian monsoon change during the LGM. Here, the Australian monsoon intensity is represented by the seasonality of precipitation, i.e., a stronger monsoon means a wetter summer and/or drier winter. Some records show wet conditions over Australia during the LGM (Ayliffe et al., 2013), while other proxies indicate drier conditions (Denniston et al., 2013; Denniston et al., 2017; DiNezio and Tierney, 2013). The isotopes from eggshell of five regions across Australia affirms that Australia becomes drier during the LGM (Miller et al., 2016), while the archaeological record showed a refugia-type hunter-gatherer response over northwest and northeast Australia during the LGM (Williams et al., 2013), indicating that these areas might have had a wetter summer and were therefore

79　preferred by people as refugia. The synthesis by the OZ-INTIMATE (Australian INTIMATE,

80　INTegration of Ice core, MArine and TErrestrial records) project (Turney et al., 2006; Petherick

81　et al., 2013) showed that the palaeoenvironment over Northern Australia during the LGM was

82　characterized by drier conditions although wet periods were also noted in the fluvial records

83　(Reeves et al., 2013a; Reeves et al., 2013b).

84　　　　The change in the Australian monsoon was inconclusive during the LGM based on proxy

85　data. Therefore, scholars started investigating the Australian monsoon change from numerical

86　simulation perspectives. The sensitivity of Australian monsoon to forcings during the late

87　Quaternary has been analyzed using simulations by Fast Ocean Atmosphere Model (Marshall

88　and Lynch, 2006, 2008). Numerical experiments have been conducted to analyze the impacts of

89　obliquity and precession with a coupled General Circulation Model (Wyrwoll et al., 2007) and

90　orbital time-scale circulation with Community Climate Model (Wyrwoll et al., 2012) on the

91　Australian monsoon. However, different models may have different responses to the same

92　external forcings, such that the simulated results may have model dependence. Multi-model

93　ensemble (MME) can reduce the model biases and therefore provide more reasonable results of

94　how and why climate system responds to the external forcing changes. The MME can also

95　provide a clearer perspective on model uncertainties.

96　　　　Yan et al (2016) thus used the multi-model ensemble approach to examine the response

97　of global monsoon to the LGM conditions. It was found that the global monsoon and most sub-

98　monsoons weakened under the LGM conditions. Some brief hypothesis was made to explain the

99　changes from global and hemispheric perspectives. The Australian monsoon was thought to be

100　strengthened due to the southward shift of the ITCZ resulted from the hemispheric thermal

101　contrast and due to the land-sea thermal contrast resulted from the land-configuration. However,

102　this simulated result of strengthened monsoon or wet condition has not been proved yet. As

103　mentioned above, it is inconclusive whether the Australian monsoon is strengthened or not

104　during the LGM, due to the limitations of proxies' and models' uncertainties. Neither model

105　outputs nor proxy records provide a "true" record of the LGM, as proxy records require

106　interpretation and calibration and may be spatially incomplete, while models contain biases.

107　Therefore, model-data and inter-model comparison are needed and studies on the mechanisms

108　are required to better understand the Australian monsoon change during the LGM. Moreover,

109　some studies show that the Australian climate during the last glacial period was modulated by

110   additional mechanisms rather than simply the ITCZ（Bayon et al., 2017). Thus, single forcing

111   runs are also required to figure out the contributions of different forcings.

112   This paper investigates the Australian monsoon change during the LGM and its

113   mechanisms from both thermodynamics and dynamics perspectives, using the multi-model

114   ensemble mean derived from models in the fifth phase of the Coupled Model Intercomparison

115   Project (CMIP5) (Taylor et al., 2012) and the third phase of the Paleoclimate Modeling

116   Intercomparison Project (PMIP3) (Braconnot et al., 2012). We are also trying to quantify the

117   contributions of the thermodynamic and the dynamic processes to the Australian monsoon

118   change during the LGM. Additionally, we are applying single forcing run to test the effect of

119   land-configuration as mentioned in Yan et al. (2016). The models and experiments used in this

120   paper are introduced in Sect. 2. Section 3 describes simulated results and the physical

121   mechanisms. The comparison with proxies and other simulations is discussed in Sect. 4 and the

122   conclusions are made in Sect. 5.

123

2 Methods

125   2.1 CMIP5/PMIP3 models and experiments

126   Two experiments performed by models participating in CMIP5/PMIP3 are compared in

127   this paper: the Last Glacial Maximum Experiment (LGME) and the pre-industrial (PI) control

128   run (piControl). The models and experiments are listed in Table 1, including 7 models and 2

129   experiments.

130   The last 100 years of the LGME and the last 500 years of the piControl from each model

131   are used to calculate the model climatology. To obtain the MME, the model outputs are

132   interpolated into a fixed 2.5° (latitude) × 2.5° (longitude) grid using the bilinear interpolation

133   method.

134   The LGM external forcings and boundary conditions are listed in Table 2. More specific

135   documentation can be found on the PMIP3 website (https://pmip3.lsce.ipsl.fr). Compared with

136   the PI, during the LGM the Southern Hemisphere (SH) low latitudes (30°S-EQ) receive more

137   insolation from January to August and less from August to December. The NH low latitudes

138   (EQ-30°N) receive less insolation from June to October and more from November to May (Fig.

S1). Due to the decreased sea level, the landmasses expand during the LGM. A land bridge forms between Indochina and western Indonesia, and the Arafura Sea between New Guinea and Australia is closed and becomes landmass (Fig. S2).

To illustrate the robust changes simulated by the different models, the signal-to-noise ratio (S2N) test is used. The S2N is defined by the ratio of the absolute mean of the MME (as the signal) to the averaged absolute deviation of the individual model against the MME (as the noise) (Yan et al., 2016). In the following sections, we only consider the areas in which the S2N ratio exceeds one when we examine the differences between the LGME and the piControl derived from the MME.

The models contributed to CMIP5 have been evaluated in the previous studies to have better performance than those in the CMIP Phase 3 (CMIP3) in simulating the Australian monsoon precipitation seasonality or seasonal cycle (Jourdain et al., 2013; Brown et al., 2016), which is used to represent the Australian monsoon intensity in this study. However, we need to keep in mind that there are large uncertainties in model simulations, which require careful model-data comparison and inter-model comparison.

2.2 NESM model and experiments

To isolate the impacts of land-sea configuration change, two additional sensitivity experiments are conducted using a newly developed fully coupled Earth system model, the Nanjing University of Information Science and Technology Earth System model version 1 (NESM v1, Cao et al., 2015). One is the piControl run (NESM_PI), using the same PI boundary conditions as the PMIP3 protocol. The other is the land sea configuration sensitivity run (NESM_LSM), using the same PI boundary conditions as the NESM_PI but with the LGM land sea configuration. The two experiments are run 500 years after spin-up, and the last 100 years are used.

2.3 Decomposition method

For attribution of precipitation changes, we use a simplified relation based on the linearized equation of moisture budget used in the previous works (Chou et al., 2009; Seager et al., 2010; Huang et al., 2013; Endo and Kitoh, 2014; Liu et al., 2016). Considering a quasi-equilibrium state, the vertical integrated moisture conservation can be written as:

6

168
$$-\int_{1000}^{0} \nabla \cdot (q\vec{v})dp = P - E \quad (1)$$

169 where q is specific humidity, $\vec{v}$ is horizontal velocity, p is pressure, P is precipitation, and E is

170 surface evaporation. Since the water vapor is concentrated in the lower troposphere, the vertical

171 integrated total column moisture divergence can be approximately replaced by the integration

172 from the surface to 500 hPa. Define the Δ (.) as the change from PI to the LGM, i.e.,

173
$$\Delta(.) = (.)\text{LGM} - (.)\text{PI} \quad (2)$$

174 Then the precipitation change ΔP can be calculated as follows:

175
$$\Delta P = -\int_{p1000}^{p500} \Delta(q \cdot \nabla\vec{v})dp - \int_{p1000}^{p500} \Delta(\vec{v} \cdot \nabla q)\, dp + \Delta E \quad (3)$$

176 To further simplify the equation, we use $-\omega_{500}$ to represent vertical integrated $\nabla\vec{v}$, and q at the

177 surface to represent vertical integrated specific humidity (Huang et al., 2013). Thus, the

178 precipitation change (ΔP) can be represented as

179
$$\Delta P \propto \overline{\omega}_{500} \cdot \Delta q + \overline{q} \cdot \Delta\omega_{500} + \Delta E - \Delta T_{adv} \quad (4)$$

180 where $\overline{\omega}_{500}$ is 500 hPa vertical velocity in PI, $\overline{q}$ is surface specific humidity in PI, ΔT_{adv} is the

181 changes due to the moisture advection ($\int_{p0}^{p500} \Delta(\vec{v} \cdot \nabla q)\, dp$).

182   The first term in the right-hand side of (4) ($\overline{\omega}_{500} \cdot \Delta q$) represents thermodynamic effect

183 (due to the change of q), and the second term ($\overline{q} \cdot \Delta\omega_{500}$) represents dynamic effect (due to the

184 change of circulation).

185 2.4 Monsoon domain

186   The monsoon domain is defined following the hydroclimate definition, i.e., a contrast

187 between wet summer and dry winter (Wang and Ding 2008). The monsoon domain is defined by

188 the area where the annual range (local summer minus local winter) exceeds 2.0 mm/day, and the

189 local summer precipitation exceeds 55% of the annual total precipitation. Here in the SH,

190 summer means November to March and winter means May to September. Since the domains

191 derived from different models are different, and the changes of domain are also different, we use

192 the fixed domain derived from the merged Climate Prediction Center Analysis of Precipitation

193 (CMAP, Xie and Arkin, 1997) and Global Precipitation Climatology Project (GPCP, Huffman et

194 al., 2009) data.

195   Note that the monsoon domain is shown to give a general view of precipitation change.

196 But the monsoon domain is not the purpose of this study, i.e. the following analyses are not

197 based on the monsoon domain.

198

199 **3 Results**

200   We define the difference of precipitation rate between austral summer (DJF) and austral

201 winter (JJA) as the annual range, i.e. the seasonality, to measure the monsoonality of the

202 Australian monsoon. An increased annual range (or seasonality) means a strengthened

203 monsoonality. Unlike the South African and South American monsoon regions (not shown), the

204 monsoonality of the Australian monsoon derived from the seven models' multi-model ensemble

205 (7MME) is strengthened during the LGM (Fig. 1a). This amplified annual range is the result of

206 increased precipitation in austral summer and decreased precipitation in austral winter (Fig. 1b).

207 Note that the largest decrease in precipitation occurs from April to July (late autumn to early

208 winter), not exactly in austral winter; and the largest increase of precipitation occurs in

209 November and December (ND), i.e., austral early summer. Since the amount of autumn–winter

210 reduction of precipitation exceeds the increased precipitation in early summer, the annual mean

211 precipitation over the strengthened annual range region decreases (by 0.36 mm/day). In

212 summary, while the total annual precipitation decreases in the LGM, the annual range (or the

213 seasonality) of the Australian monsoon rainfall is amplified due to seasonal redistribution of the

214 precipitation, especially the drying in austral autumn (April–May) and winter (JJA) over

215 Australia.

216   Although there are model biases, most of the models (except MPI-ESM-P) simulate an

217 enhanced annual range (or seasonality/monsoonality) in the central Australian monsoon region

218 (20°S-5°S, 120°E-145°E) (Table 3 and Fig. 1c). Most of the models (except CNRM-CM5 and

219 MPI-ESM-P) also simulate an increased summer precipitation over that region. All the models

220 simulate decreased precipitation from April to September (Fig. 1c). On the other hand, the

221 simulated annual mean precipitation is decreased in most models, except GISS-E2-R. The model

222 uncertainties will be discussed later in Sec. 4.

223 3.1 Reasons for the decreased precipitation during the LGM in austral winter (JJA)

224   During the LGM, the lower GHG concentration and the large ice-sheets are the primary

225   causes for the decreased global temperature and humidity. The global surface specific humidity

226   is reduced by 2 g/kg (or 20 %) in JJA during the LGM, compared with the PI. For the SH

227   monsoon regions, the surface specific humidity is reduced more over the Australian monsoon

228   region than over the other two monsoon regions of South Africa and South America (Fig. 2).

229   As suggested by the Clausius–Clapeyron relation (C-C relation), one degree of

230   temperature decrease would lead to about a 7 % decrease in the saturation water vapor (Held and

231   Soden, 2006), or roughly the same scale of decrease in the low tropospheric specific humidity. If

232   the circulation, evaporation and advection remains unchanged, the precipitation should also be

233   reduced by 7 % with regard to the equation (4). During the LGM, the simulated near surface air

234   temperature over the central Australian monsoon region (20°S-5°S, 120°E-145°E) decreases

235   significantly by 2.5 K in JJA, which implies a decreased precipitation of about 17 % resulted

236   from the C-C relation. However, the simulated precipitation in the LGM is reduced by 1.45

237   mm/day or 44 % comparing to the PI, which is far beyond the value suggested by the

238   thermodynamic effect (approximately 17 %). This suggests that the majority of the reduction in

239   winter precipitation is due to the changes of the rest terms of equation (4), including the

240   circulation change (dynamics), the evaporation change and the change due to the advection term.

241   The changes of each terms show that the circulation change plays a dominant role in the

242   precipitation change over Australia (Fig. S3). The change due to the evaporation is also

243   important. The change due to the advection term is negligible.

244   The change of the surface wind field shows a strengthened divergence pattern over the

245   Australian monsoon region (Fig. 3a, vector), which is consistent with the strengthened

246   descending flow over the Australian monsoon region (Fig. 4) and thus the reduced precipitation

247   (Fig. 3a, shading). The JJA mean near surface air temperature shows that the land is cooler than

248   the adjacent ocean around northern Australia (Fig. 5a), which illustrates a strengthened land–sea

249   thermal contrast because the land cools more than the ocean surface during the LGM. This

250   strengthened land–sea thermal contrast leads to a higher sea-level pressure (SLP) over land and

251   lower SLP over ocean in general (Fig. 5b, shading), and thus the outflows from land (Fig. 5b,

252   vector). The geopotential height at 850 hPa also shows the relative pattern that matches the wind

253   change (Fig. S4a). The difference of divergence/convergence field (Fig. 5c) also indicates that

254   the divergence at 850 hPa over northern Australia is strengthened during the LGM. The vertical

9

velocity at 500 hPa over the central Australian monsoon region (20°S-5°S, 120°E-145°E) illustrates that the descending flow strengthened by about 48 %.

In conclusion, both the dynamic process (increased subsidence) and the thermodynamic process (reduced water vapor content) contribute to the drier winter in the Australian monsoon region, but the local dynamic process play a dominant role in the reduction of Australian winter precipitation.

3.2 Why the precipitation increased in austral early summer (ND)

During ND, the LGM minus PI surface wind difference field shows a strengthened convergence pattern over the central northern Australian monsoon region (Fig. 6a, vector), which is consistent with the increased precipitation (Fig. 6a, shading). The vertical velocity at 500 hPa also shows a strengthened ascending flow over this area (Fig. 7). The increased precipitation over the central Australian monsoon region is clearly against the thermodynamic effects of the low GHG concentration and the presence of the ice-sheets, which tend to reduce the precipitation. The 2-m air temperature is decreased by 2.2 K and the surface specific humidity is reduced by 2.6 g/kg (or 16.0 %) over the Australian monsoon region (Fig. 8). The precipitation would decrease by 15.4 % according to the thermodynamic effect without the circulation change. However, the precipitation over the Australian monsoon region is increased by about 13.0 %. Therefore, the changes in dynamic processes must induce a 29 % increase of precipitation, so that the net increase in precipitation reaches 13 %.

There is a cyclonic wind anomaly associated with an anomalous low pressure over the northwest Australia (Fig. 6a and Fig. 9b, vector), accompanied by a strengthened low-level convergence (Fig. 9c), which favors increased precipitation in the Australian monsoon region. The change of the moisture transport (moisture flux) also indicates increased moisture transport into northern Australia (not shown). The cyclonic vorticity in northwest Australia is partially caused by the enhanced strong low-level westerlies that prevail north of Australia.

We now seek to determine why there is a strengthened low-level westerly with maximum over north of Australia. We first consider the temperature change. The ND mean 2-m air temperature during the LGM shows that the two enlarged landmasses over the Indo-Pacific warm pool region (resulting from the lower sea level) change differently (Fig. 9a). It is cooler over the northwest landmass (western Indonesia–Indochina) and relatively warmer over the

285 southeast landmass (eastern Indonesia–northern Australia). This temperature variation forms a

286 southeast–northwest temperature gradient (Fig. 9a, Fig. S5a, S5b), accompanied by a northwest–

287 southeast SLP gradient (Fig. 9b, Fig. S5c, S5d). The northwest–southeast pressure gradient is

288 stronger in the geopotential height change at 850 hPa (Fig. S4b). The high pressure in the

289 western Indonesia–Indochina is a part of the larger scale enhanced winter monsoon over the

290 South China Sea. This enhanced winter monsoon flows cross the equator from the NH to the SH

291 and turn into strong westerlies due to deflection induced by the Coriolis force. The 850 hPa

292 convergence strengthens over the Australian monsoon region (Fig. 9c), and the corresponding

293 ascending motion at 500 hPa also increases over the Australian monsoon region.

294   Another reason for circulation change is the sea surface temperature (SST) gradient

295 change. The SST anomaly in ND shows a warmer Western Pacific and cooler Eastern Indian

296 Ocean pattern (Fig. 10), indicating a westward temperature gradient (Fig. S5e), and thus an

297 eastward pressure gradient which, in the equatorial region, can directly enhance westerly winds

298 near the northern Australian monsoon region (Fig. 9b). Li et al. (2012) also found that a cold

299 state of the Wharton Basin (100°E–130°E, 20°S–5°S) was accompanied by anomalous westerlies

300 and cyclonic circulation anomalies in the Australian monsoon region, which were associated

301 with a strong tropical Australian summer monsoon and enhanced rainfall over northeast

302 Australia.

303   In summary, during ND, the enlarged land area due to sea-level drop enhances the land–

304 sea thermal contrast, and forms a northwest–southeast thermal contrast which induces low

305 pressure over northern Australia but high pressure over the adjacent ocean and the Indochina–

306 western Indonesia, leading to the enhanced convergence over northern Australia and thus the

307 increased early summer monsoon rainfall. The SST gradients between the warm equatorial

308 western Pacific and the relatively cool eastern Indian Ocean during the pre-summer monsoon

309 season also contribute to the strengthened equatorial westerlies and the cyclonic wind anomaly

310 over northern Australia. These dynamic mechanisms have a positive contribution to the early

311 summer precipitation. The thermodynamic effects have negative contribution to the precipitation

312 change, but with smaller magnitude. Therefore, the early summer precipitation over northern

313 Australia increases. We can also tell from the changes of the decomposed terms that the

314 dynamics plays much more important role in the precipitation change over Australia, especially

315 the distribution pattern (Fig. S6). The impacts of evaporation and advection terms are small.

11

4 Discussion

The intensification of the Australian monsoon in this study is measured by the enhanced seasonal difference (or the seasonality) of precipitation, and is particularly attributed to the decreased austral winter precipitation. This is consistent with the reconstructed results by Mohtadi et al. (2011), which indicated that it was not significantly drier in austral summer during the LGM, while the winter monsoon was as weak as the modern period. Whereas the annual mean precipitation is decreased, which means the Australian monsoon would be weakened during the LGM when it is measured by the annual mean precipitation. The modeling study by DiNezio et al. (2013) suggested a decreasing rainfall across northern Australia during the LGM, consistent with the proxy synthesis by stalagmite (Denniston et al., 2017). The decreased rainfall in their work represents the annual mean precipitation, which is also consistent with our work. On the other hand, the increased rainfall in austral summer in this study is consistent with what has been revealed in the reconstructed work by Liu et al. (2015), which found intense austral summer precipitation over Papua New Guinea and North Australia in LGM. The decreased annual mean precipitation and the intensified seasonality of precipitation over the Australian monsoon region are in agreement with the synthesis from the simulated result by Tharammal et al. (2013) using a set of experiments.

For the forcings and mechanisms of the Australian monsoon change during the LGM, there are large changes in four external forcings during the LGM, including the insolation change resulting from the orbital change, the land–sea configuration change, the GHG change and the presence of ice-sheets. The lower GHG concentrations and the presence of ice-sheets are likely to be contributors to the thermodynamic effect leading to the reduced water vapor and thus the decreased rainfall both in austral winter and early summer. The enlarged landmasses over western Indonesia and northeastern Australia are essential to the local dynamic processes that influence the rainfall. The low obliquity and high precession during the LGM may be another factor that can affect the rainfall (Liu et al., 2015). However, the impact of the insolation change caused by the orbital change remains unknown.

During the LGM, the insolation over tropical region increases from December to June and decreases from July to November relative to the present day (Fig. 11a). In the annual

12

346 variation, the precipitation responds to the lower tropospheric moisture convergence. The

347 moisture change depends on the temperature change while the circulation change depends on the

348 surface temperature gradients change. The change of the surface temperature lags insolation

349 changes because the ocean and land surfaces have heat capacity (thermal inertial). In other

350 words, insolation is a heating rate which equals to temperature change (tendency) but not the

351 temperature itself. Thus the precipitation change would lag the insolation change by about two

352 months, due to the ocean–atmosphere interaction without other processes. However, the

353 simulated Australian monsoon precipitation is decreased from March to September and increased

354 from November to February (Fig. 11b), quite different from what it would be (i.e., decrease from

355 September to January and increase from February to August). This indicates that the insolation

356 change might have little effect on the Australian monsoon precipitation. Meanwhile, the

357 insolation over SH is increased during the LGM from April to August, when Australia is in late

358 autumn and winter. An increased insolation might make land warmer than ocean thus against the

359 climatology (i.e. cooler land and warmer ocean in winter). However, the simulated surface

360 temperature reduces more over Australia than the adjacent oceans (Fig. 5a). On the other hand,

361 the synthesis of Wyrwoll et al. (2007) and Liu et al. (2015) indicates that the strong convergence

362 rain belt (ITCZ) stays in the north during those times with low obliquity and high precession,

363 which is a little more northerly than that stays in our study. These mean that the effect of orbital

364 change and thus the insolation change might be suppressed by other factors.

365   Moreover, the paleoclimate records suggested that it was dry and cool in the Indo-Pacific

366 Warm Pool region during the LGM (Xu et al., 2010). The simulated SST is consistent with the

367 reconstructions. Although in the early austral summer, over the Indian Ocean warm pool, it is

368 cooler over the SH, while over the Pacific warm pool, it is cooler over the NH (Fig. S7). Such

369 anomalous SST asymmetry may favor the southward shift of the ITCZ over Australia and the

370 southwest Pacific, which might be related to the enhanced austral summer monsoon

371 precipitation. However, the 7MME shows no significant ITCZ shift during the LGM, particularly

372 over the central Australian monsoon region (Fig. S8). The reconstructions and simulations by

373 McGee et al. (2014) and Mohtadi et al. (2014) also suggested that there was no significant shift

374 of ITCZ position during the LGM.

375   Therefore, it is the local dynamical processes, instead of the large-scale circulation such

376 as the position of the ITCZ induced by the NH-SH thermal contrast, that might be the key factor

377 influencing the early summer mean precipitation change over the Australian monsoon region

378 during the LGM. To test this hypothesis, we compared the results from the two additional runs,

379 the NESM_PI and the NESM_LSM. The changes of the ND mean precipitation and wind field at

380 1000 hPa between the NESM_LSM and the NESM_PI are similar to the changes derived from

381 the 7MME, i.e. the precipitation is increased and the convergence is strengthened over northern

382 Australia (Fig. 12a). The changes of the 2-m air temperature, SLP and 850 hPa wind field (Fig.

383 12b, c) are also similar to those results in the 7MME (Fig. 9). It is also cooler over the northwest

384 landmass (western Indonesia–Indochina) and relatively warmer over the southeast landmass

385 (eastern Indonesia–northern Australia) (Fig. 12b). This temperature variation is also

386 accompanied by a northwest–southeast SLP gradient and the strengthened cross equatorial flow

387 converging to north Australia (Fig. 12c). This sensitivity simulation confirms that the local

388 dynamical processes induced by the land sea configuration are essential to the Australian

389 monsoonality change.

390 Although the 7MME simulates a strengthened Australian monsoonality, there are

391 uncertainties among individual models. The most notable uncertainty is the increased austral

392 summer (DJF) precipitation. Five out of the 7 models simulate increased DJF mean precipitation

393 over the Australian monsoon region during the LGM (CCSM4, GISS-E2-R, IPSL-CM5A-LR,

394 MIROC-ESM and MRI-CGCM3), while the other two simulate decreased precipitation (CNRM-

395 CM5 and MPI-ESM-P) (Fig. 13), especially over the land area. The wind field at 850hPa

396 geopotential height shows a cyclonic anomaly pattern over northern Australia in the five models

397 (Fig. 14a), accompanied with a strengthened ascending flow (not shown). While in the other two

398 models, there is no cyclonic wind anomaly over Australia region (Fig. 14b), and the ascending

399 flow is weakened (not shown). The different changes of wind field indicate the different

400 precipitation responses to the LGM boundary conditions in the two model groups.

401 The austral spring and summer mean 2m-air temperature and SST also change differently

402 in these two model groups. The main differences are located over the tropic Pacific Ocean and

403 the North Atlantic Ocean. It is cooler over high-latitude North Atlantic Ocean in the five models,

404 whereas warmer in the two models, mainly in the austral spring (Fig. 15a, 15b). In the austral

405 summer, there is an eastern Pacific El Nino-like patter in the five models, while there is a

406 Central-Pacific El Nino (CP-El Nino) like pattern in the two models (Fig. 15c, 15d). Studies have

14

407 shown that the CP-El Nino is related to the Asian-Australian monsoon system (Yu et al. 2009),

408 and would lead to a markedly decreased precipitation in December (Taschetto et al. 2009).

409 Therefore, the different SST responses over the Pacific Ocean and the North Atlantic

410 Ocean in austral spring and summer in different models might be the key factor that leads to

411 different wind anomalies and thus different Australian monsoon precipitation changes. Note that

412 the resolution of land configuration in each model might not be the key factor that affects the

413 SST gradient over the eastern Indian Ocean and western Pacific Ocean (Fig. S9).

414

5 Conclusions

416 The global mean temperature and water vapor have an overall decrease under the LGM

417 forcings (lower GHG and large ice-sheets). Nevertheless, the simulated Australian monsoon

418 seasonality derived from CMIP5/PMIP3 multi-model ensemble has a distinctive amplification

419 (or the monsoonality is intensified) against the weakened global monsoons elsewhere during the

420 LGM. This study then investigated the possible reasons for this strengthened Australian

421 monsoonality from both thermodynamic and dynamic perspectives.

422 The conclusions are as follows:

423 1) The Australian monsoon seasonality is strengthened as a result of the enhanced

424 seasonal difference between austral summer and winter, i.e., the increased early

425 summer (ND) mean rainfall and the reduced winter (JJA) mean rainfall. Both the

426 dynamic processes and thermodynamic effects contribute to the precipitation change;

427 however, the dynamic processes have a much stronger contribution than the

428 thermodynamic effects.

429 2) The Australian winter (JJA mean) precipitation derived from 7MME is decreased

430 during the LGM relative to the preindustrial control experiment. The dynamic

431 processes, induced by the enhanced land–ocean thermal contrast, contribute more to the

432 decreased rainfall through the strengthened divergence over northern Australia (Fig.

433 16a), whereas the thermodynamic effect (i.e., the reduced atmospheric water vapor due

434 to the lower temperature induced by the lower GHGs and the presence of ice-sheets)

435 and evaporation have moderate contributions.

15

3)   For the increased precipitation in early summer (ND) in the 7MME, the local dynamic processes have a positive contribution and the thermodynamic effect has a negative contribution. Both the decomposition method and the sensitivity simulations show that the dynamic effect plays most important role for the increased rainfall. The local dynamic processes are mainly induced by the northwest–southeast thermal contrast between Indochina–western Indonesia and northeastern Australia. The eastern Indian Ocean–western Pacific Ocean thermal gradient also contributes to these processes (Fig. 16b).

4)   The sensitivity simulation illustrates that the change in circulation over Australia is very likely to be rooted in the enlarged landmasses over the Indochina–western Indonesia and New Guinea, and northern Australia. Another factor contributes to the circulation change might be the asymmetric change between western Pacific Ocean and eastern Indian Ocean. These have critical impacts on the thermal gradients that induce changes in the low-level circulation pattern and convergence/divergence.

Note that models have uncertainties, i.e. not all the models simulate an intensified seasonality of Australian monsoon. The different SST responses over Pacific Ocean and Atlantic Ocean in different models to the same external forcings are essential for the model uncertainties. More model-data comparison and inter-model comparison are required to better understand the model-data disagreement and improve confidence in model results.

Our results are based on the equilibrium simulation, representing a mean state of the Australian monsoon change and its possible mechanisms during the LGM. More simulations with single forcing (such as the SST asymmetry change, the insolation change) are required to further understand the effect of each factor and to specifically quantify the contribution of each forcing to the Australian monsoon change.

References

Ayliffe, L. K., Gagan, M. K., Zhao, J. X., Drysdale, R. N., Hellstrom, J. C., Hantoro, W. S., Griffiths, M. L., Scott-Gagan, H., St Pierre, E., Cowley, J. A., and Suwargadi, B. W.: Rapid interhemispheric climate links via the Australasian monsoon during the last deglaciation, Nat Commun, 4, 2908, 10.1038/ncomms3908, 2013.

Bayon, G., De Deckker, P., Magee, J. W., Germain, Y., Bermell, S., Tachikawa, K., and Norman, M. D.: Extensive wet episodes in Late Glacial Australia resulting from high-latitude forcings, Scientific Reports, 7, 44054, 10.1038/srep44054, 2017.

Braconnot, P., Otto-Bliesner, B., Harrison, S. P., and al, e.: Results of PMIP2 coupled simulations of the Mid-Holocene and Last Glacial Maximum – Part 2: feedbacks with emphasis on the location of the ITCZ and mid- and high latitudes heat budget, Climate of the Past, 3, 2007.

Braconnot, P., Harrison, S. P., Kageyama, M., Bartlein, P. J., Masson-Delmotte, V., Abe-Ouchi, A., Otto-Bliesner, B., and Zhao, Y.: Evaluation of climate models using palaeoclimatic data, Nature Climate Change, 2, 417-424, 10.1038/nclimate1456, 2012a.

Braconnot, P., Harrison, S. P., Otto-Bliesner, B., Abe-Ouchi, A., Jungclaus, J., and Peterschmitt, J. Y.: The Paleoclimate Modeling Intercomparison Project contribution to CMIP5, CLIVAR Exchanges, 56, 15-19, 2012b.

Broccoli, A. J., Dahl, K. A., and Stouffer, R. J.: Response of the ITCZ to Northern Hemisphere cooling, Geophysical Research Letters, 33(1), L01702, 10.1029/2005gl024546, 2006.

Brown, J. R., Moise, A. F., Colman, R., and Zhang, H.: Will a Warmer World Mean a Wetter or Drier Australian Monsoon? Journal of Climate, 29, 4577-4596, 10.1175/jcli-d-15-0695.1, 2016.

Cao, J., Wang, B., Xiang, B., Li, J., Wu, T., Fu, X., Wu, L., and Min, J.: Major modes of short-term climate variability in the newly developed NUIST Earth System Model (NESM), Advances in Atmospheric Sciences, 32, 585-600, 10.1007/s00376-014-4200-6, 2015.

Chou, C., Neelin, J. D., Chen, C.-A., and Tu, J.-Y.: Evaluating the "Rich-Get-Richer" Mechanism in Tropical Precipitation Change under Global Warming, Journal of Climate, 22, 1982-2005, 10.1175/2008jcli2471.1, 2009.

505 Cui, X. P.: Quantitative diagnostic analysis of surface rainfall processes by surface rainfall
506   equation. Chinese Journal of Atmospheric Sciences, 33(2), 375–387, 2009.

507 De Deckker, P., Barrows, T. T., and Rogers, J.: Land–sea correlations in the Australian region:
508   post-glacial onset of the monsoon in northwestern Western Australia, Quaternary Science
509   Reviews, 105, 181-194, 10.1016/j.quascirev.2014.09.030, 2014.

510 Denniston, R. F., Wyrwoll, K.-H., Asmerom, Y., Polyak, V. J., Humphreys, W. F., Cugley, J.,
511   Woods, D., LaPointe, Z., Peota, J., and Greaves, E.: North Atlantic forcing of millennial-
512   scale Indo-Australian monsoon dynamics during the Last Glacial period, Quaternary
513   Science Reviews, 72, 159-168, 10.1016/j.quascirev.2013.04.012, 2013.

514 Denniston, R. F., Asmerom, Y., Polyak, V. J., Wanamaker, A. D., Ummenhofer, C. C.,
515   Humphreys, W. F., Cugley, J., Woods, D., and Lucker, S.: Decoupling of monsoon activity
516   across the northern and southern Indo-Pacific during the Late Glacial, Quaternary Science
517   Reviews, 176, 101-105, 10.1016/j.quascirev.2017.09.014, 2017.

518 DiNezio, P. N., Timmermann, A., Tierney, J. E., Jin, F.-F., Otto-Bliesner, B., Rosenbloom, N.,
519   Mapes, B., Neale, R., Ivanovic, R. F., and Montenegro, A.: The climate response of the
520   Indo-Pacific warm pool to glacial sea level, Paleoceanography, 31, 866-894,
521   10.1002/2015PA002890, 2016.

522 DiNezio, P. N., Clement, A., Vecchi, G. A., Soden, B., Broccoli, A. J., Otto-Bliesner, B. L., and
523   Braconnot, P.: The response of the Walker circulation to Last Glacial Maximum forcing:
524   Implications for detection in proxies, Paleoceanography, 26, n/a-n/a,
525   10.1029/2010pa002083, 2011.

526 DiNezio, P. N., and Tierney, J. E.: The effect of sea level on glacial Indo-Pacific climate, Nature
527   Geoscience, 6, 485-491, 10.1038/ngeo1823, 2013.

528 Donohoe, A., Marshall, J., Ferreira, D., and McGee, D.: The Relationship between ITCZ
529   Location and Cross-Equatorial Atmospheric Heat Transport: From the Seasonal Cycle to
530   the Last Glacial Maximum, Journal of Climate, 26, 3597-3618, 10.1175/jcli-d-12-00467.1,
531   2013.

19

532   Endo, H., and Kitoh, A.: Thermodynamic and dynamic effects on regional monsoon rainfall
533   changes in a warmer climate, Geophysical Research Letters, 41, 1704-1711,
534   10.1002/2013gl059158, 2014.

535   Eroglu, D., McRobie, F. H., Ozken, I., Stemler, T., Wyrwoll, K. H., Breitenbach, S. F., Marwan,
536   N., and Kurths, J.: See-saw relationship of the Holocene East Asian-Australian summer
537   monsoon, Nat Commun, 7, 12929, 10.1038/ncomms12929, 2016.

538   Hargreaves, J. C., Annan, J. D., Ohgaito, R., Paul, A., and Abe-Ouchi, A.: Skill and reliability of
539   climate model ensembles at the Last Glacial Maximum and mid-Holocene, Climate of the
540   Past, 9, 811-823, 10.5194/cp-9-811-2013, 2013.

541   Harrison, S. P., Bartlein, P. J., Brewer, S., Prentice, I. C., Boyd, M., Hessler, I., Holmgren, K.,
542   Izumi, K., and Willis, K.: Climate model benchmarking with glacial and mid-Holocene
543   climates, Climate Dynamics, 43, 671-688, 10.1007/s00382-013-1922-6, 2014.

544   Held, I. M., and Soden, B. J.: Robust responses of the hydrological cycle to global warming,
545   Journal of Climate, 19, 5686-5699, 2006.

546   Hewitt, C., Broccoli, A. J., Mitchell, J. F. B., and Stouffer, R.: A coupled model study of the last
547   glacial maximum: Was part of the North Atlantic relatively warm? Geophys. Res. Lett., 28,
548   1571-1574, 2001.

549   Huang, P., Xie, S.-P., Hu, K., Huang, G., and Huang, R.: Patterns of the seasonal response of
550   tropical rainfall to global warming, Nature Geoscience, 6, 357-361, 10.1038/ngeo1792,
551   2013.

552   Huffman, G. J., Adler, R. F., Bolvin, D. T., and Gu, G.: Improving the global precipitation
553   record: GPCP Version 2.1, Geophysical Research Letters, 36, 10.1029/2009gl040000, 2009.

554   Jiang, D., Tian, Z., Lang, X., Kageyama, M., and Ramstein, G.: The concept of global monsoon
555   applied to the last glacial maximum: A multi-model analysis, Quaternary Science Reviews,
556   126, 126-139, 10.1016/j.quascirev.2015.08.033, 2015.

557   Jourdain, N. C., Gupta, A. S., Taschetto, A. S., Ummenhofer, C. C., Moise, A. F., and Ashok, K.:
558   The Indo-Australian monsoon and its relationship to ENSO and IOD in reanalysis data and
559   the CMIP3/CMIP5 simulations, Climate Dynamics, 41, 3073-3102, 10.1007/s00382-013-
560   1676-1, 2013.

561 Kuhnt, W., Holbourn, A., Xu, J., Opdyke, B., De Deckker, P., Rohl, U., and Mudelsee, M.:
562   Southern Hemisphere control on Australian monsoon variability during the late deglaciation
563   and Holocene, Nat Commun, 6, 5916, 10.1038/ncomms6916, 2015.

564 Li, J., Feng, J., and Li, Y.: A possible cause of decreasing summer rainfall in northeast Australia,
565   International Journal of Climatology, 32, 995-1005, 10.1002/joc.2328, 2012.

566 Liu, F., Chai, J., Wang, B., Liu, J., Zhang, X., and Wang, Z.: Global monsoon precipitation
567   responses to large volcanic eruptions, Sci Rep, 6, 24331, 10.1038/srep24331, 2016.

568 Liu, Y., Lo, L., Shi, Z., Wei, K. Y., Chou, C. J., Chen, Y. C., Chuang, C. K., Wu, C. C., Mii, H.
569   S., Peng, Z., Amakawa, H., Burr, G. S., Lee, S. Y., DeLong, K. L., Elderfield, H., and Shen,
570   C. C.: Obliquity pacing of the western Pacific Intertropical Convergence Zone over the past
571   282,000 years, Nat Commun, 6, 10018, 10.1038/ncomms10018, 2015.

572 Marshall, A. G., and Lynch, A. H.: Time-slice analysis of the Australian summer monsoon
573   during the late Quaternary using the Fast Ocean Atmosphere Model, Journal of Quaternary
574   Science, 21, 789-801, 10.1002/jqs.1063, 2006.

575 Marshall, A. G., and Lynch, A. H.: The sensitivity of the Australian summer monsoon to climate
576   forcing during the late Quaternary, Journal of Geophysical Research, 113,
577   10.1029/2007jd008981, 2008.

578 McGee, D., Donohoe, A., Marshall, J., and Ferreira, D.: Changes in ITCZ location and cross-
579   equatorial heat transport at the Last Glacial Maximum, Heinrich Stadial 1, and the mid-
580   Holocene, Earth and Planetary Science Letters, 390, 69-79, 10.1016/j.epsl.2013.12.043,
581   2014.

582 Miller, G. H., Fogel, M. L., Magee, J. W., and Gagan, M. K.: Disentangling the impacts of
583   climate and human colonization on the flora and fauna of the Australian arid zone over the
584   past 100 ka using stable isotopes in avian eggshell, Quaternary Science Reviews, 151, 27-
585   57, 10.1016/j.quascirev.2016.08.009, 2016.

586 Mohtadi, M., Prange, M., Oppo, D. W., De Pol-Holz, R., Merkel, U., Zhang, X., Steinke, S., and
587   Lückge, A.: North Atlantic forcing of tropical Indian Ocean climate, Nature, 509, 76,
588   10.1038/nature13196, 2014.

589 Petherick, L., Bostock, H., Cohen, T. J., Fitzsimmons, K., Tibby, J., Fletcher, M. S., Moss, P.,
590   Reeves, J., Mooney, S., Barrows, T., Kemp, J., Jansen, J., Nanson, G., and Dosseto, A.:
591   Climatic records over the past 30 ka from temperate Australia – a synthesis from the Oz-
592   INTIMATE workgroup, Quaternary Science Reviews, 74, 58-77,
593   10.1016/j.quascirev.2012.12.012, 2013.

594 Reeves, J. M., Barrows, T. T., Cohen, T. J., Kiem, A. S., Bostock, H. C., Fitzsimmons, K. E.,
595   Jansen, J. D., Kemp, J., Krause, C., Petherick, L., and Phipps, S. J.: Climate variability over
596   the last 35,000 years recorded in marine and terrestrial archives in the Australian region: an
597   OZ-INTIMATE compilation, Quaternary Science Reviews, 74, 21-34,
598   10.1016/j.quascirev.2013.01.001, 2013a.

599 Reeves, J. M., Bostock, H. C., Ayliffe, L. K., Barrows, T. T., De Deckker, P., Devriendt, L. S.,
600   Dunbar, G. B., Drysdale, R. N., Fitzsimmons, K. E., Gagan, M. K., Griffiths, M. L.,
601   Haberle, S. G., Jansen, J. D., Krause, C., Lewis, S., McGregor, H. V., Mooney, S. D., Moss,
602   P., Nanson, G. C., Purcell, A., and van der Kaars, S.: Palaeoenvironmental change in
603   tropical Australasia over the last 30,000 years – a synthesis by the OZ-INTIMATE group,
604   Quaternary Science Reviews, 74, 97-114, 10.1016/j.quascirev.2012.11.027, 2013b.

605 Rojas, M.: Sensitivity of Southern Hemisphere circulation to LGM and $4 \times CO_2$ climates,
606   Geophysical Research Letters, 40, 965-970, 10.1002/grl.50195, 2013.

607 Seager, R., Naik, N., and Vecchi, G. A.: Thermodynamic and Dynamic Mechanisms for Large-
608   Scale Changes in the Hydrological Cycle in Response to Global Warming*, Journal of
609   Climate, 23, 4651-4668, 10.1175/2010jcli3655.1, 2010.

610 Taylor, K. E., Stouffer, R. J., and Meehl, G. A.: An Overview of CMIP5 and the Experiment
611   Design, Bulletin of the American Meteorological Society, 93, 485-498, 10.1175/bams-d-11-
612   00094.1, 2012.

613 Tharammal, T., Paul, A., Merkel, U., and Noone, D.: Influence of Last Glacial Maximum
614   boundary conditions on the global water isotope distribution in an atmospheric general
615   circulation model, Climate of the Past, 9, 789-809, 10.5194/cp-9-789-2013, 2013.

616 Turney, C. S. M., Haberle, S., Fink, D., Kershaw, A. P., Barbetti, M., Barrows, T. T., Black, M.,
617   Cohen, T. J., Corrège, T., Hesse, P. P., Hua, Q., Johnston, R., Morgan, V., Moss, P.,

618   Nanson, G., van Ommen, T., Rule, S., Williams, N. J., Zhao, J. X., D'Costa, D., Feng, Y.

619   X., Gagan, M., Mooney, S., and Xia, Q.: Integration of ice-core, marine and terrestrial

620   records for the Australian Last Glacial Maximum and Termination: a contribution from the

621   OZ INTIMATE group, Journal of Quaternary Science, 21, 751-761, 10.1002/jqs.1073,

622   2006.

623 Wang, B., and Ding, Q.: Global monsoon: Dominant mode of annual variation in the tropics,

624   Dynamics of Atmospheres and Oceans, 44, 165-183, 10.1016/j.dynatmoce.2007.05.002,

625   2008.

626 Wang, P. X., Wang, B., Cheng, H., Fasullo, J., Guo, Z., Kiefer, T., and Liu, Z.: The global

627   monsoon across time scales: Mechanisms and outstanding issues, Earth-Science Reviews,

628   10.1016/j.earscirev.2017.07.006, 2017.

629 Williams, A. N., Ulm, S., Cook, A. R., Langley, M. C., and Collard, M.: Human refugia in

630   Australia during the Last Glacial Maximum and Terminal Pleistocene: a geospatial analysis

631   of the 25–12 ka Australian archaeological record, Journal of Archaeological Science, 40,

632   4612-4625, 10.1016/j.jas.2013.06.015, 2013.

633 Wyrwoll, K.-H., Liu, Z., Chen, G., Kutzbach, J. E., and Liu, X.: Sensitivity of the Australian

634   summer monsoon to tilt and precession forcing, Quaternary Science Reviews, 26, 3043-

635   3057, 10.1016/j.quascirev.2007.06.026, 2007.

636 Wyrwoll, K.-H., Hopwood, J. M., and Chen, G.: Orbital time-scale circulation controls of the

637   Australian summer monsoon: a possible role for mid-latitude Southern Hemisphere forcing?

638   Quaternary Science Reviews, 35, 23-28, 10.1016/j.quascirev.2012.01.003, 2012.

639 Xie, P., and Arkin, P.: Global precipitation: a 17-year monthly analysis based on Gauge

640   Obseravations, satellite estimates, and numerical model outputs, Bulletin of the American

641   Meteorological Society, 78, 2539-2558, 1997.

642 Xu, J., Kuhnt, W., Holbourn, A., Regenberg, M., and Andersen, N.: Indo-Pacific Warm Pool

643   variability during the Holocene and Last Glacial Maximum, Paleoceanography, 25,

644   10.1029/2010pa001934, 2010.

645 Yan, M., Wang, B., and Liu, J.: Global monsoon change during the Last Glacial Maximum: a

646   multi-model study, Climate Dynamics, 47, 359-374, 10.1007/s00382-015-2841-5, 2016.

647

648

649

650
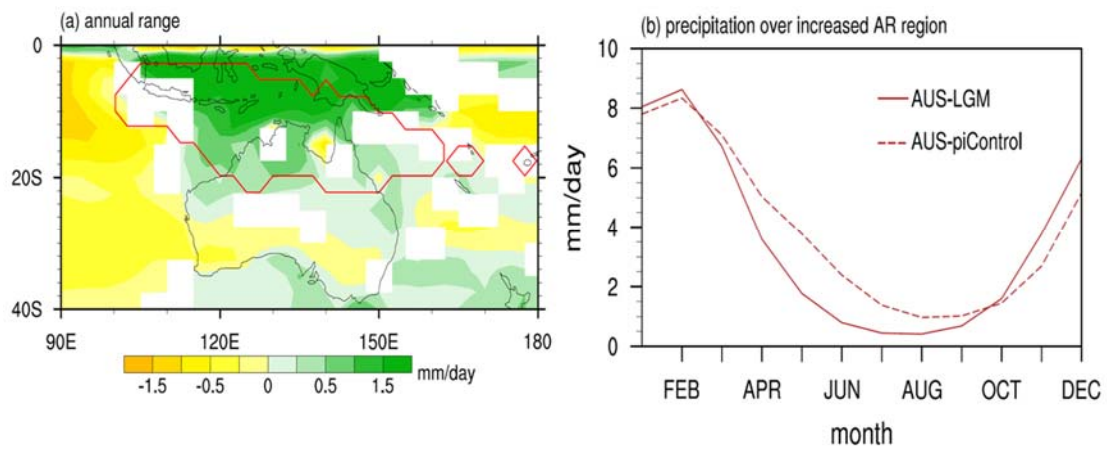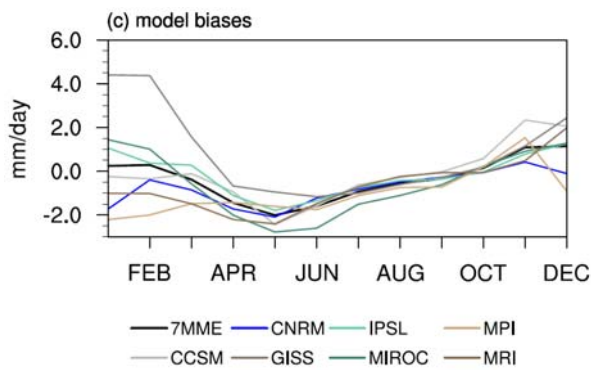
Figure 1 (**a**) Spatial distribution of changes in the annual range (AR) of precipitation measured by the difference between LGME and piControl, (**b**) seasonal distribution of the precipitation in the increased AR area (20°S-5°S, 120°E-145°E), and (c) seasonal distribution of the precipitation differences in the increased AR area derived from 7 MME (black line) and each model (colored lines). The red solid line in (**a**) encloses the Australian monsoon rainfall domain. The dashed (solid) line in (**b**) denotes the seasonal distribution of precipitation derived from the piControl (LGME) run. Only those areas where signal-to-noise ratio exceeds one are plotted in (**a**).

658
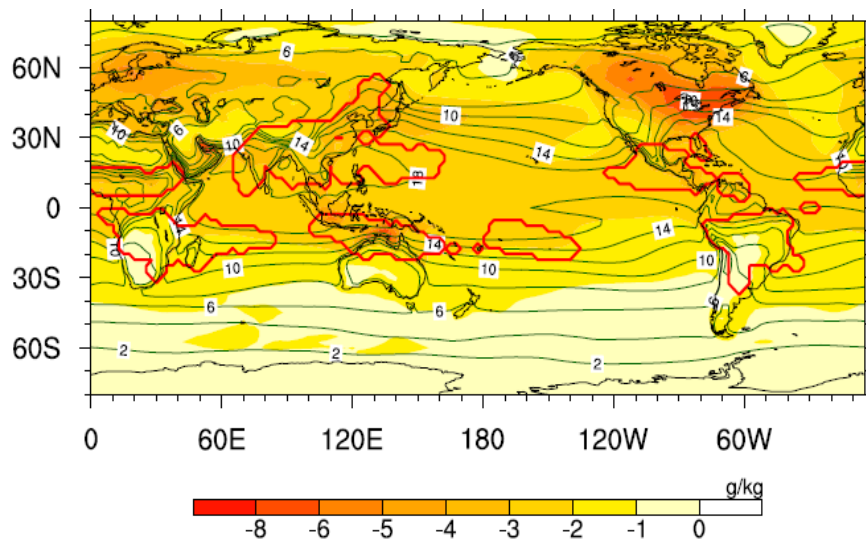
Figure 2 Difference of JJA mean surface specific humidity between LGME and piControl (shaded). The green contours denote the climatology derived from piControl. The red lines enclose the monsoon domains. Only those areas where signal-to-noise ratio exceeds one are plotted.

665

666
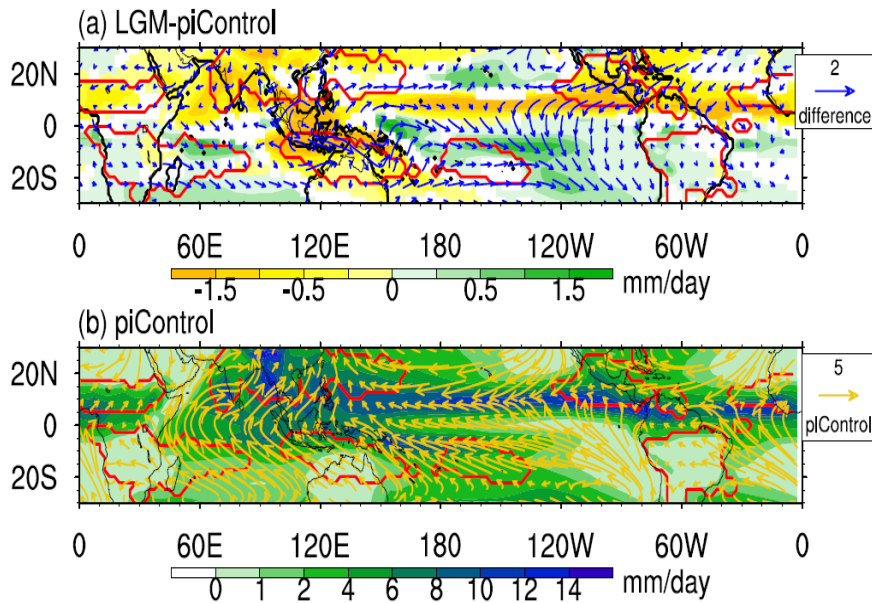
Figure 3 (**a**) JJA mean precipitation (shading) difference and surface wind (vectors) difference between LGME and piControl, and (**b**) the climatology of JJA mean precipitation (shading) and surface wind (vectors) derived from piControl. The red lines enclose the monsoon domains. The thick black lines in (**a**) denote the coastal lines in LGME provided by CMIP5/PMIP3, and the thin black lines denote the coastal lines in piControl. Only those areas where signal-to-noise ratio exceeds one are plotted in (**a**).

673

27

674

675
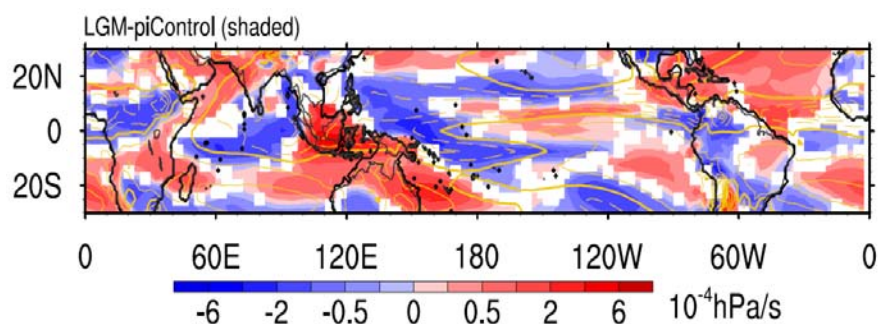
Figure 4 The difference of JJA mean vertical velocity at 500 hPa between LGME and piControl (in shading) and the corresponding climatology derived from piControl (yellow contours). The thick black lines denote the coastal lines in LGME provided by CMIP5/PMIP3, and the thin black lines denote the coastal lines in piControl. Only those areas where signal-to-noise ratio exceeds one are plotted in the difference pattern.

681
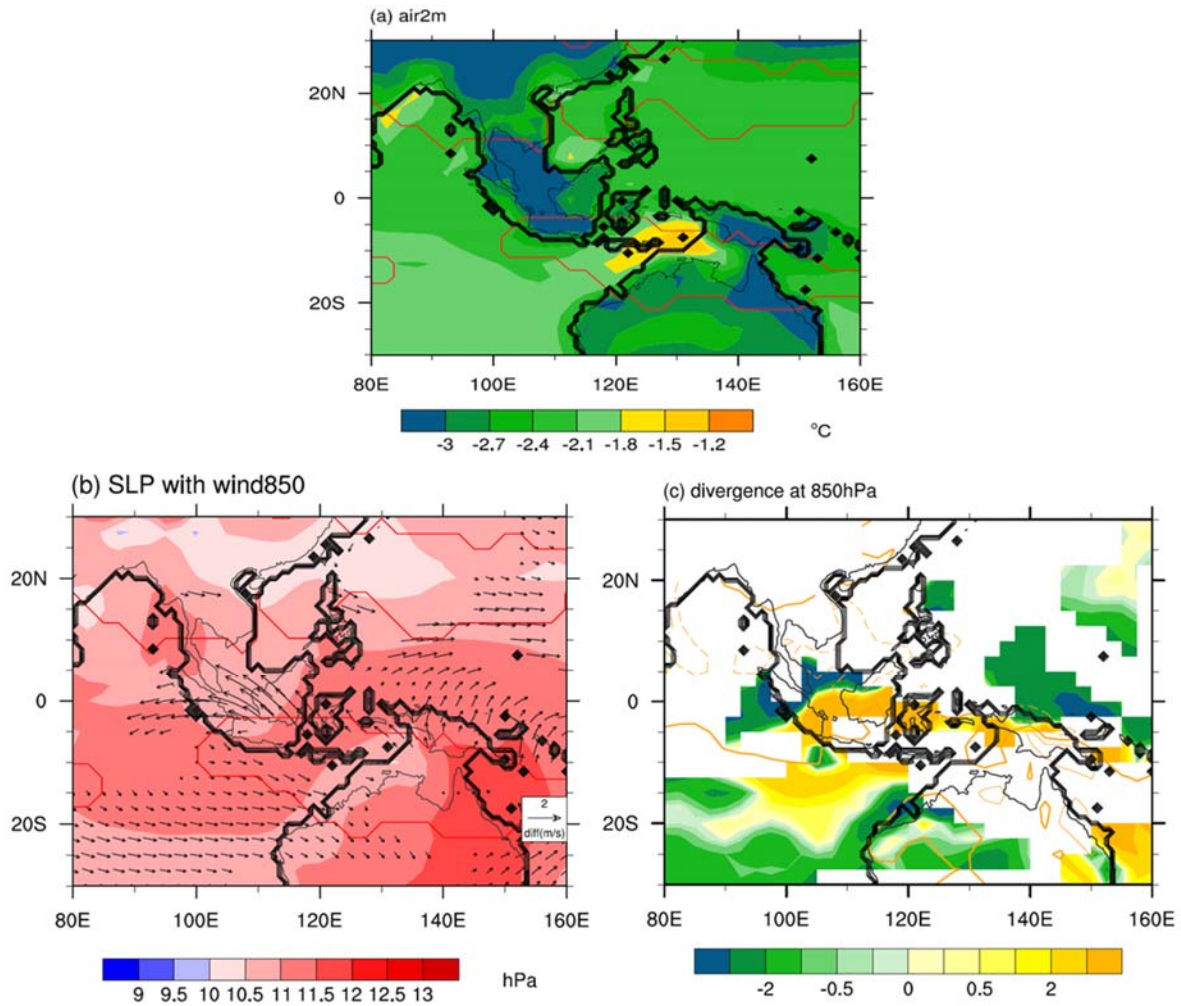
Figure 5 JJA mean (**a**) surface air temperature, (**b**) sea level pressure (shading) with 850 hPa wind (vector), and (**c**) 850 hPa divergence differences between LGME and piControl. The red lines in (**a**) and (**b**) enclose the monsoon domains. The orange lines in (**c**) represent the climatology derived from piControl. The thick black lines denote the coastal lines in LGME provided by CMIP5/PMIP3, and the thin black lines denote the coastal lines in piControl. Only those areas where signal-to-noise ratio exceeds one are plotted.

(a) ND mean precp diff (LGM-piControl)

(b) ND mean precp (piControl climatology)
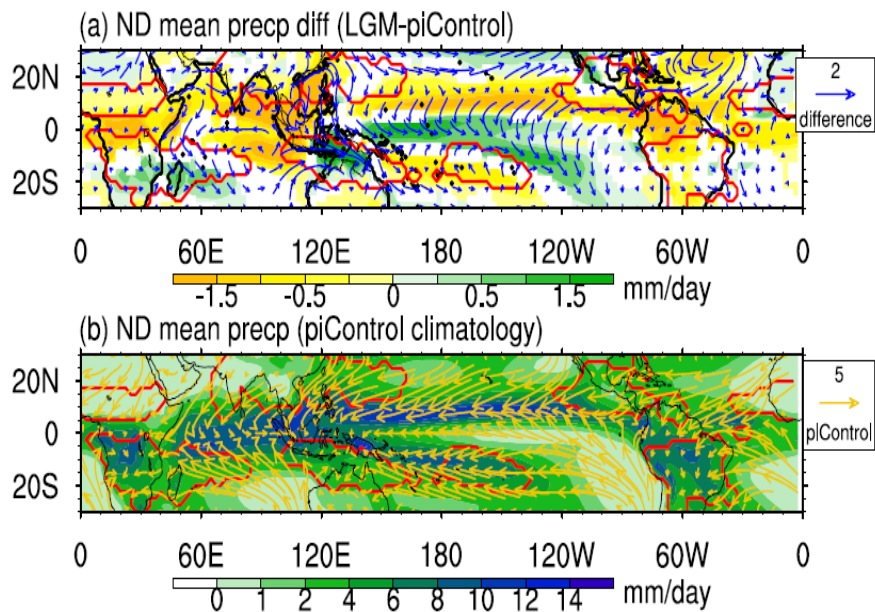
Figure 6 (**a**) ND mean precipitation (shading) difference and surface wind (vectors) difference between LGME and piControl, and (**b**) the climatology of ND mean precipitation (shading) and surface wind (vectors) derived from piControl. The red lines enclose the monsoon domains. The thick black lines in (**a**) denote the coastal lines in LGME provided by CMIP5/PMIP3, and the thin black lines denote the coastal lines in piControl. Only those areas where signal-to-noise ratio exceeds one are plotted in (**a**).

698

699
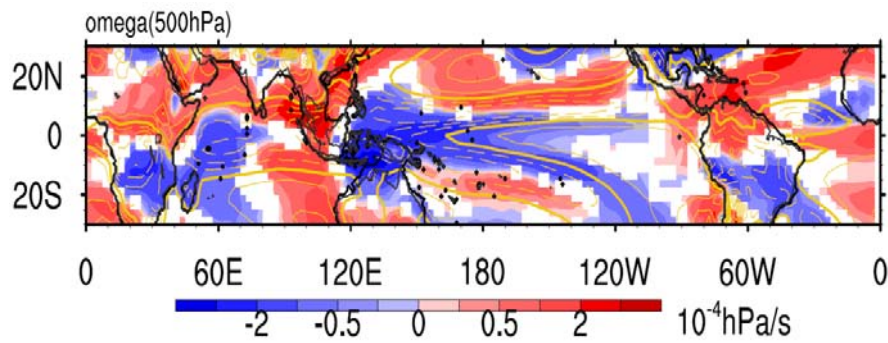
700 **Figure 7** The difference of the ND mean vertical velocity at 500 hPa between LGME and

701 piControl (in shading) and the corresponding climatology derived from piControl (yellow

702 contours). The thick black lines denote the coastal lines in LGME provided by CMIP5/PMIP3,

703 and the thin black lines denote the coastal lines in piControl. Only those areas where signal-to-

704 noise ratio exceeds one are plotted in the difference pattern.

705

Figure 8 Difference of ND mean surface specific humidity between LGME and piControl (shaded). The green contours denote the climatology derived from piControl. The red lines enclose the monsoon domains. Only those areas where signal-to-noise ratio exceeds one are plotted.
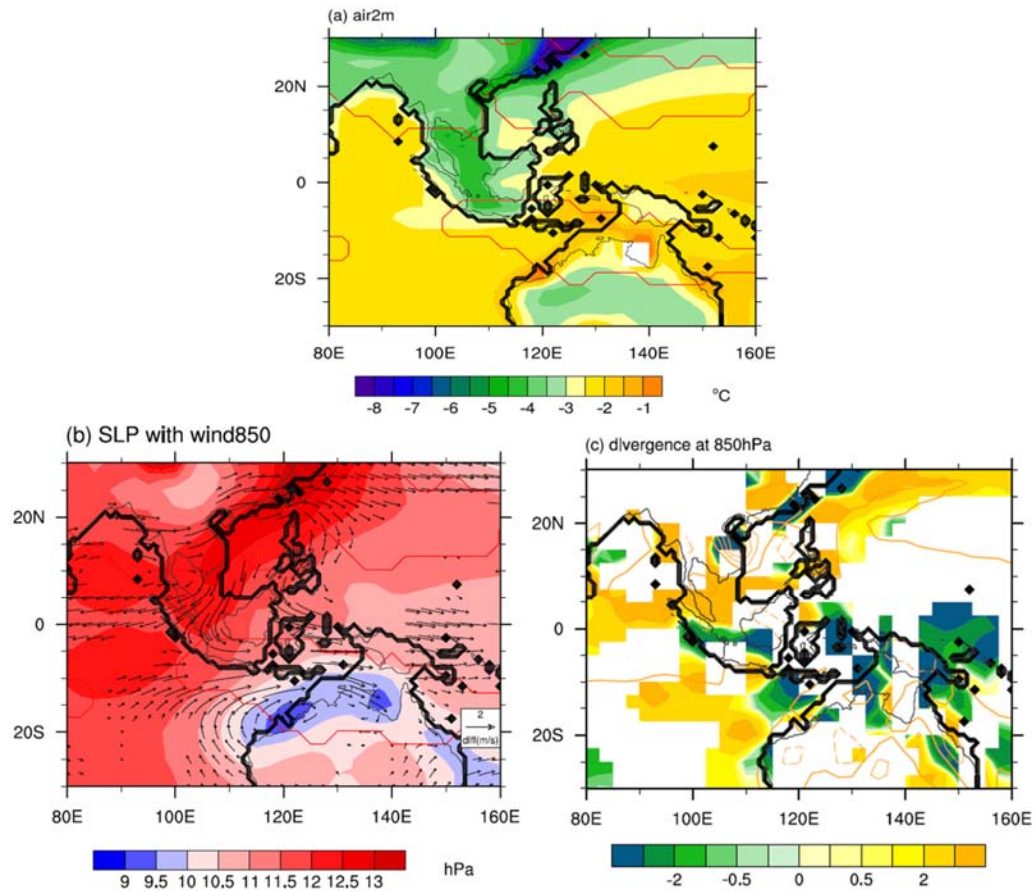
Figure 9 ND mean (**a**) surface air temperature, (**b**) sea level pressure (shading) with 850 hPa wind (vector), and (**c**) 850 hPa divergence difference between LGME and piControl (shading). The red lines in (**a**) and (**b**) enclose the monsoon domains. The orange lines in (**c**) represents the climatology derived from piControl. The thick black lines denote the coastal lines in LGME provided by CMIP5/PMIP3, and the thin black lines denote the coastal lines in piControl. Only those areas where signal-to-noise ratio exceeds one are plotted.
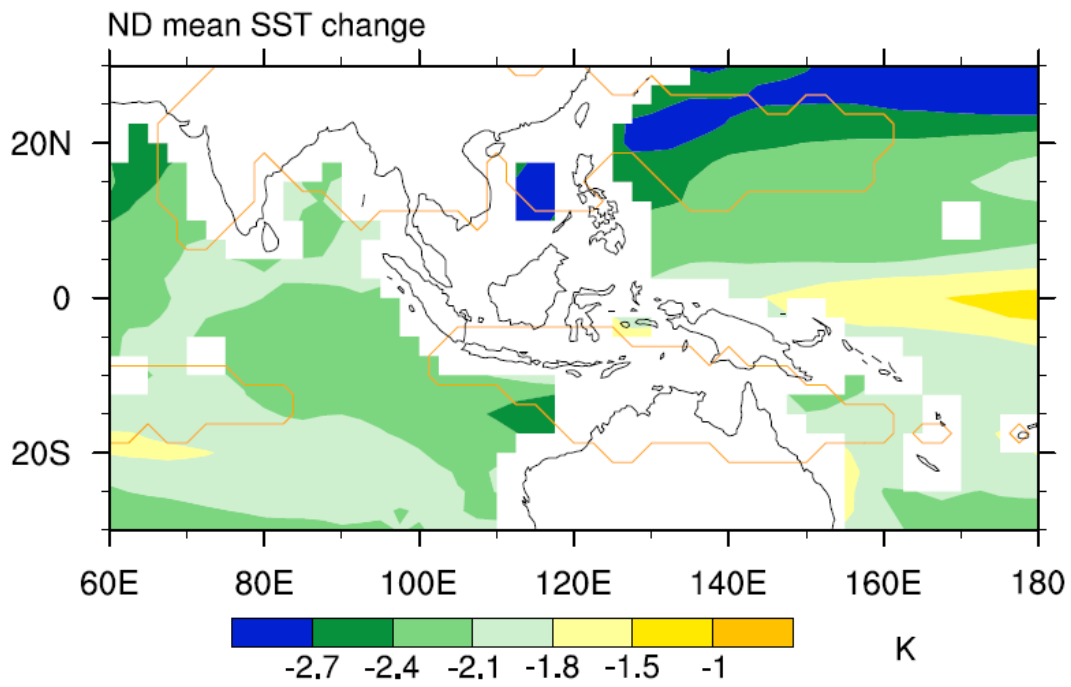
Figure 10 ND mean SST difference between LGME and piControl. The red lines enclose the monsoon domains. Only those areas where signal-to-noise ratio exceeds one are plotted.

(a) insolation change (LGM-PI)

(b) precip chagne over increased AR region
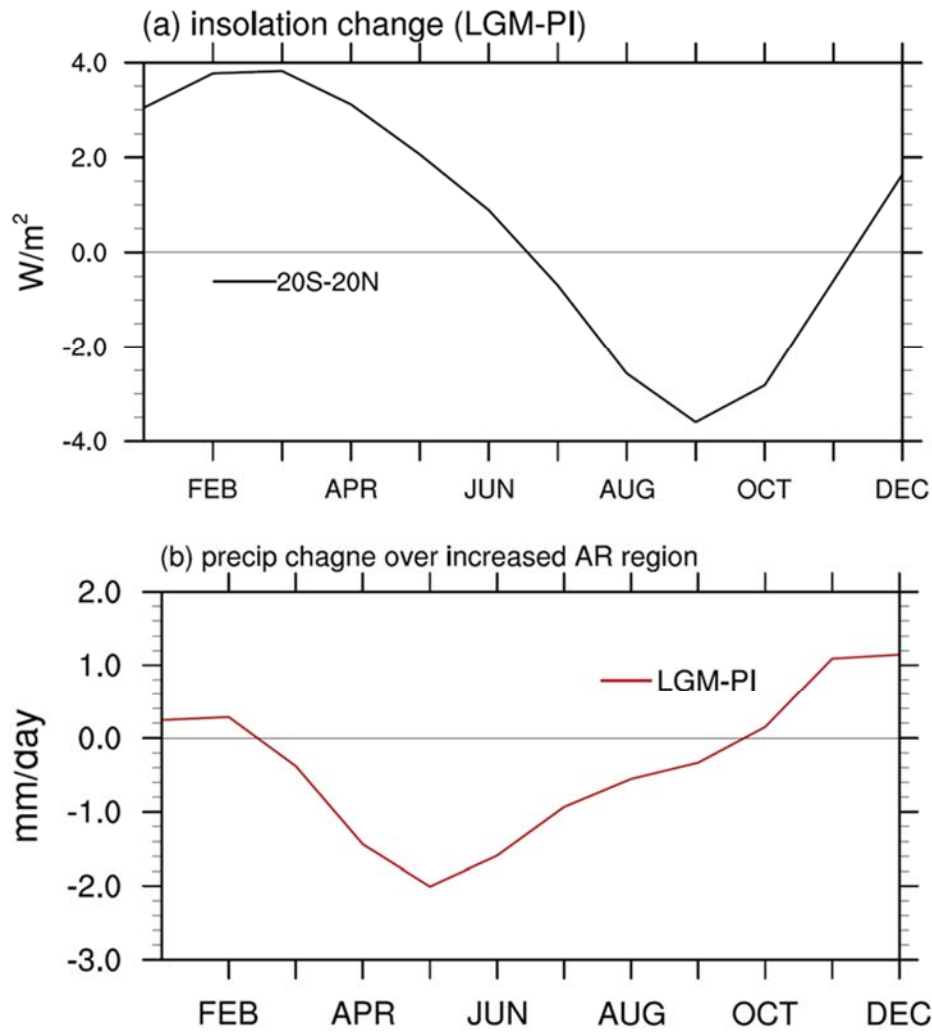
724

725 **Figure 11** Seasonal distribution of (**a**) insolation change between 20°S and 20°N, and (**b**)

726 precipitation change over the increased AR region as indicated in Fig. 1b (20°S-5°S, 120°E-

727 145°E). The changes are calculated by the LGM value minus the PI value.

728

729

730

731

732

733

734
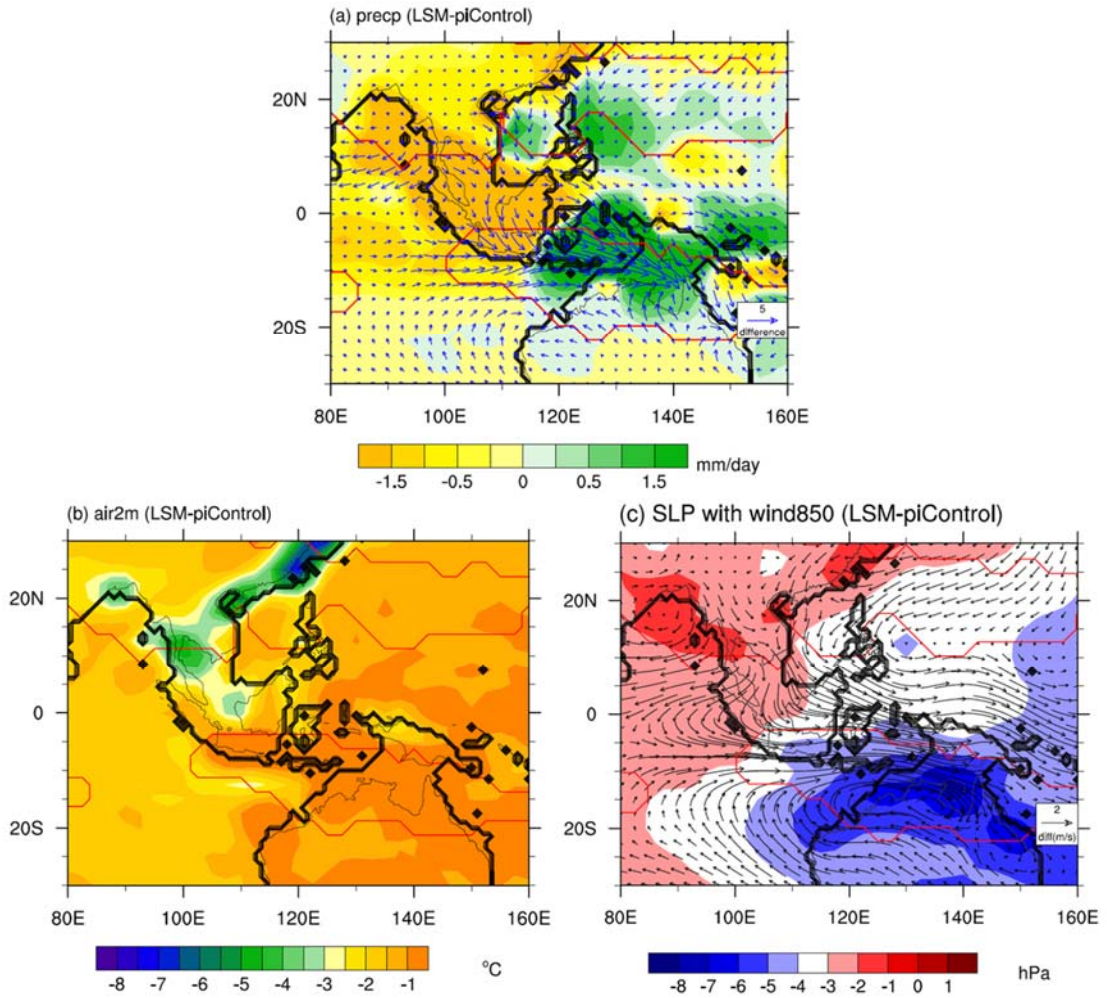
Figure 12 ND mean (a) precipitation (shading) with 1000 hPa wind (vector), (b) surface air temperature, and (c) sea level pressure (shading) with 850 hPa wind (vector) difference between the NESM_LSM and the NESM_PI. The red lines enclose the monsoon domains. The thick black lines denote the coastal lines in NESM_LSM, and the thin black lines denote the coastal lines in NESM_PI.
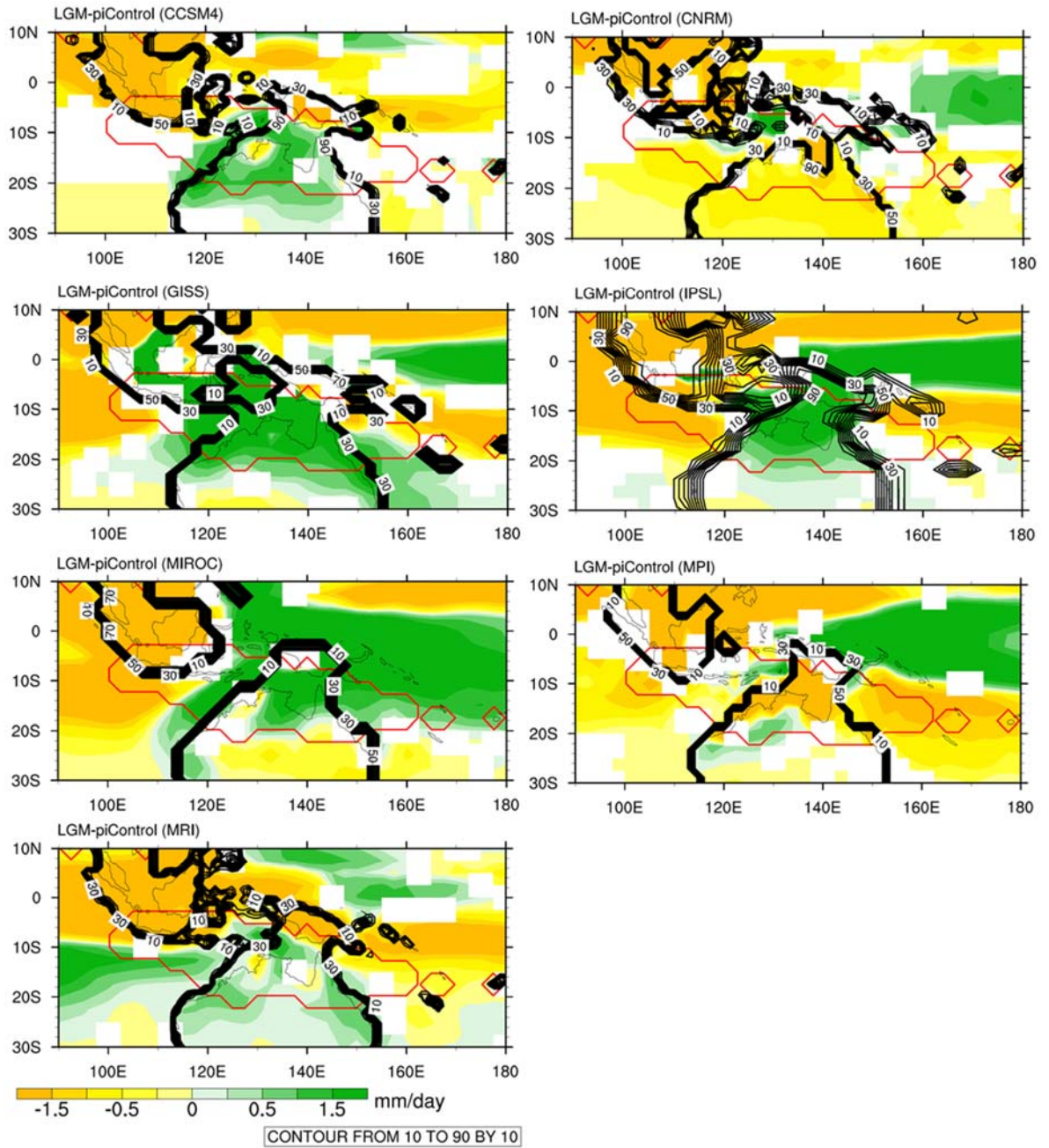
Figure 13 DJF mean precipitation differences between LGME and piControl derived from each model. The red lines enclose the monsoon domains. The dark black lines show the land area fraction used for the LGME in each model. Only those areas where signal-to-noise ratio exceeds one are plotted.

748

749

(a) LGM - piControl (5models)

(b) LGM - piControl (2models)

750
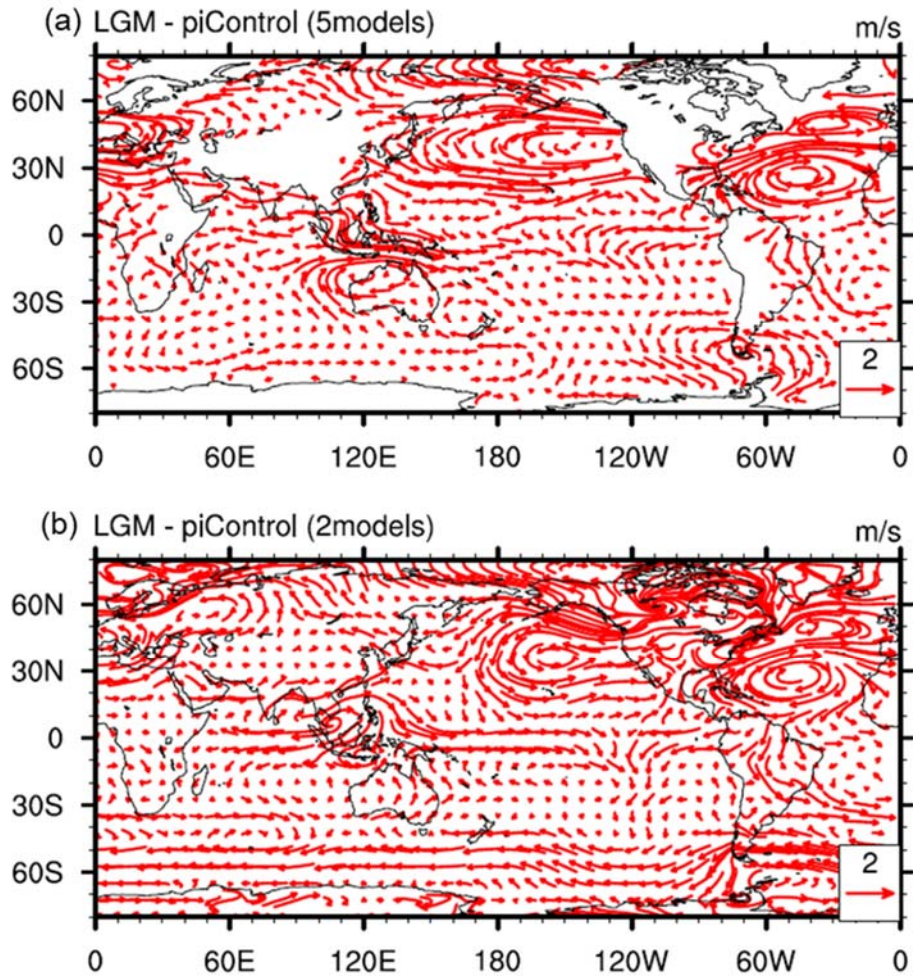
Figure 14 DJF mean 850hPa wind differences between LGME and piControl derived from (a) the five models and (b) the two models. Only those areas where signal-to-noise ratio exceeds one are plotted.

754
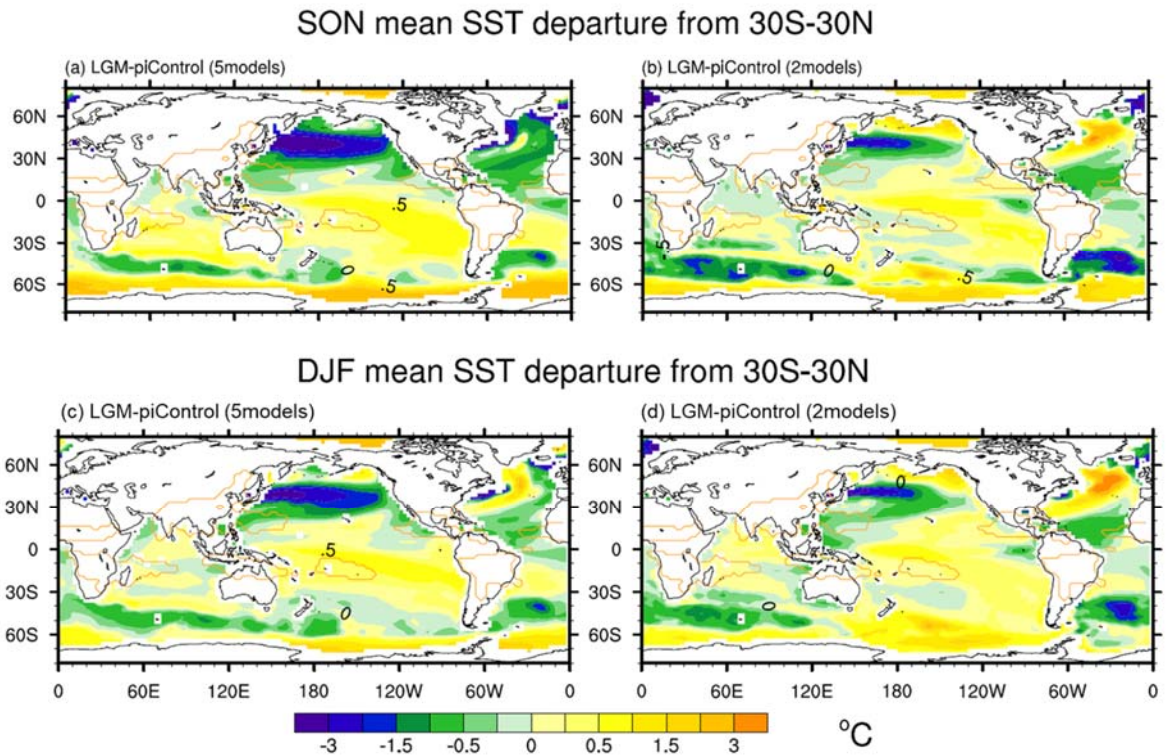
Figure 15 SON mean (a)-(b) and DJF mean (c)-(d) SST differences between LGME and piControl derived from (a), (c) the five models and (b), (d) the two models. Only those areas where signal-to-noise ratio exceeds one are plotted. The area average of tropical (30°S-30°N) SST change is distracted to make it clearer to illustrate the regional differences.

762

763
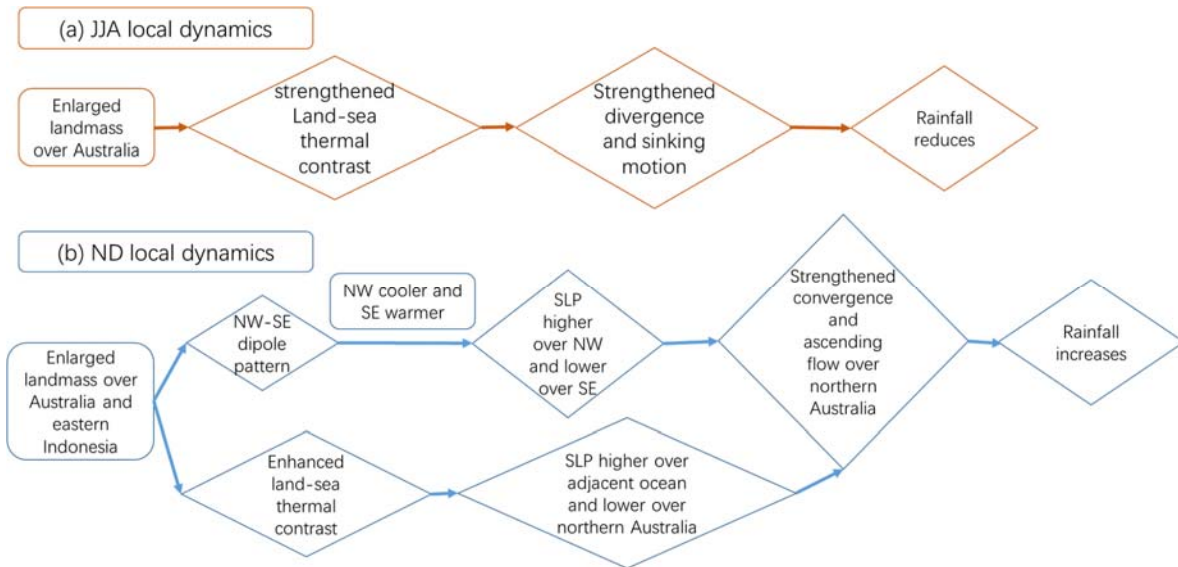
Figure 16 Mechanisms of Australian monsoon precipitation change (**a**) in JJA, and (**b**) in ND
during the LGM, in the local dynamics perspective.

766

767
768

Table 1 CMIP5/PMIP3 models and experiments used in this study.

Model	Institution	piControl Time span (years)	LGME Time span (years)	Spatial resolution for atmospheric module Lon × Lat Grids	Spatial resolution for oceanic module Lon × Lat Grids
CCSM4	National Centre for Atmospheric Research (NCAR)	501	101	288 × 192	320×384
CNRM-CM5	Centre National de Recherches Meteorologiques/Centre Europeen de Recherche et Formation Avancees en Calcul Scientifique (CNRM-CERFACS)	850	200	256 × 128	362×292
GISS-E2-R	NASA Goddard Institute for Space Studies (NASA GISS)	1200	100	144 × 90	288×180
IPSL-CM5A-LR	Institute Pierre-Simon Laplace (IPSL)	1000	200	96 × 95	182×149
MIROC-ESM	Atmosphere and Ocean Research Institute, University of Tokyo, National Institute for Environmental studies, and Japan Agency for Marine-Earth Science and Technology	531	100	128 × 64	256×192
MPI-ESM-P	Max Planck Institute for Meteorology	1156	100	196 × 98	256×220
MRI-CGCM3	Meteorological Research Institute (MRI)	500	100	320 × 160	364×368

772

773 **Table 2** Main changed boundary conditions used for the piControl and LGME experiments.

	piControl	LGME
Orbital parameters	Eccentricity = 0.016724	Eccentricity = 0.018994
	Obliquity = 23.446°	Obliquity = 22.949°
	Angular precession = 102.04°	Angular precession = 114.42°
Trace gases	CO_2 = 280 ppm	CO_2 = 185 ppm
	CH_4 = 650 ppb	CH_4 = 350 ppb
	N_2O = 270 ppb	N_2O = 200 ppb
Ice sheets	Modern	Provided by ICE-6G v2 (Peltier, 2009)
Land surface elevation and coastlines	Modern	Provided by PMIP3

774

775

776 **Table 3** Annual mean, austral summer (DJF) mean and annual range of precipitation change

777 over the region of (20°S-5°S, 120°E-145°E). The area averaged value is calculated based on

778 the areas where S2N ratio exceed one.

Model	Annual mean (mm/day)	Summer mean (mm/day)	Annual range (mm/day)
CCSM4	-0.14	0.49	1.36
CNRM-CM5	-0.78	-0.74	0.12
GISS-E2-R	0.79	3.74	4.66
IPSL-CM5A-LR	-0.17	0.90	1.82
MIROC-ESM	-0.53	1.25	3.17
MPI-ESM-P	-1.02	-1.71	-0.52
MRI-CGCM3	-0.68	-0.01	0.85
7MME	-0.36	0.56	1.61

779